Research Article | Vol. 25, No. 23 | 13 Nov 2017 | OPTICS EXPRESS 28352

Optics EXPRESS

Overcoming the classical Rayleigh diffraction limit by controlling two-point correlations of partially coherent light sources

CHUNHAO LIANG,[1] GAOFENG WU,[2] FEI WANG,[1,5] WEI LI,[3,6] YANGJIAN CAI,[1,7] AND SERGEY A. PONOMARENKO[4]

[1]*College of Physics, Optoelectronics and Energy & Collaborative Innovation Center of Suzhou Nano Science and Technology, Soochow University, Suzhou 215006, China*
[2]*School of Physics, Northwest University, Xi'an 710069, China*
[3]*School of Physics and Telecommunication Engineering, South China Normal University, Guangzhou 510006, China*
[4]*Department of Electrical and Computer Engineering, Dalhousie University, Halifax, Nova Scotia B3J2X4, Canada*
[5]*fwang@suda.edu.cn*
[6]*liwei@m.scnu.edu.cn*
[7]*yangjiancai@suda.edu.cn*

Abstract: In classical optical imaging, the Rayleigh diffraction limit d_R is defined as the minimum resolvable separation between two points under incoherent light illumination. In this paper, we analyze the minimum resolvable separation between two points under partially coherent beam illumination. We find that the image resolution of two points can overcome the classic Rayleigh diffraction limit through manipulating the correlation function of a partially coherent source, and the image resolution, which independent of the specified positions of two points in the object plane, can in principle reach the value of $0.17d_R$. Furthermore, we carry out an experimental demonstration of sub-Rayleigh imaging of a 1951 USAF resolution target via engineering the correlation function of the illuminating beam. Our experimental results are in agreement with our theoretical predictions.

OCIS codes: (030.1640) Coherence; (030.1670) Coherent optical effects; (100.2960) Image analysis.

References and links

1. T. E. Gureyev, D. M. Paganin, A. W. Stevenson, S. C. Mayo, and S. W. Wilkins, "Generalized eikonal of partially coherent beams and its use in quantitative imaging," Phys. Rev. Lett. **93**(6), 068103 (2004).
2. Y. Cai and S. Y. Zhu, "Ghost imaging with incoherent and partially coherent light radiation," Phys. Rev. E Stat. Nonlin. Soft Matter Phys. **71**(5 Pt 2), 056607 (2005).
3. J. N. Clark, X. Huang, R. Harder, and I. K. Robinson, "High-resolution three-dimensional partially coherent diffraction imaging," Nat. Commun. **3**, 993 (2012).
4. D. P. Brown and T. G. Brown, "Partially correlated azimuthal vortex illumination: Coherence and correlation measurements and effects in imaging," Opt. Express **16**(25), 20418–20426 (2008).
5. Y. Cai, Q. Lin, and S. Zhu, "Coincidence fractional Fourier transform with entangled photon pairs and incoherent light," Appl. Phys. Lett. **86**(2), 021112 (2005).
6. B. Stoklasa, L. Motka, J. Rehacek, Z. Hradil, and L. L. Sánchez-Soto, "Wavefront sensing reveals optical coherence," Nat. Commun. **5**, 3275 (2014).
7. G. Gbur, "Partially coherent beam propagation in atmospheric turbulence [invited]," J. Opt. Soc. Am. A **31**(9), 2038–2045 (2014).
8. F. Wang, X. Liu, L. Liu, Y. Yuan, and Y. Cai, "Experimental study of the scintillation index of a radially polarized beam with controllable spatial coherence," Appl. Phys. Lett. **103**(9), 091102 (2013).
9. T. van Dijk, D. G. Fischer, T. D. Visser, and E. Wolf, "Effects of spatial coherence on the angular distribution of radiant intensity generated by scattering on a sphere," Phys. Rev. Lett. **104**(17), 173902 (2010).
10. C. Zhao, F. Wang, Y. Dong, Y. Han, and Y. Cai, "Effect of spatial coherence on determining the topological charge of a vortex beam," Appl. Phys. Lett. **101**(26), 261104 (2012).
11. X. Liu, X. Peng, L. Liu, G. Wu, C. Zhao, F. Wang, and Y. Cai, "Self-reconstruction of the degree of coherence of a partially coherent vortex beam obstructed by an opaque obstacle," Appl. Phys. Lett. **110**(18), 181104 (2017).

#307368 https://doi.org/10.1364/OE.25.028352
Journal © 2017 Received 18 Sep 2017; revised 18 Oct 2017; accepted 27 Oct 2017; published 31 Oct 2017

Optics EXPRESS

12. C. H. Gan, G. Gbur, and T. D. Visser, "Surface plasmons modulate the spatial coherence of light in Young's interference experiment," Phys. Rev. Lett. **98**(4), 043908 (2007).
13. A. Norrman, S. A. Ponomarenko, and A. T. Friberg, "Partially coherent surface plasmon polaritons," Europhys. Lett. **116**(6), 64001 (2016).
14. Y. Chen, A. Norrman, S. A. Ponomarenko, and A. T. Friberg, "Plasmon coherence determination by nanoscattering," Opt. Lett. **42**(17), 3279–3282 (2017).
15. Y. Dong, F. Wang, C. Zhao, and Y. Cai, "Effect of spatial coherence on propagation, tight focusing, and radiation forces of an azimuthally polarized beam," Phys. Rev. A **86**(1), 013840 (2012).
16. Y. Chen, S. A. Ponomarenko, and Y. Cai, "Self-steering partially coherent beams," Sci. Rep. **7**, 39957 (2017).
17. Y. Cai, Y. Chen, J. Yu, X. Liu, and L. Liu, "Generation of partially coherent beams," Prog. Opt. **62**, 157–223 (2017).
18. F. Gori and M. Santarsiero, "Devising genuine spatial correlation functions," Opt. Lett. **32**(24), 3531–3533 (2007).
19. R. Martínez-Herrero, P. M. Mejías, and F. Gori, "Genuine cross-spectral densities and pseudo-modal expansions," Opt. Lett. **34**(9), 1399–1401 (2009).
20. S. Sahin and O. Korotkova, "Light sources generating far fields with tunable flat profiles," Opt. Lett. **37**(14), 2970–2972 (2012).
21. Z. Mei and O. Korotkova, "Random sources generating ring-shaped beams," Opt. Lett. **38**(2), 91–93 (2013).
22. Y. Chen, J. Gu, F. Wang, and Y. Cai, "Self-splitting properties of a Hermite-Gaussian correlated Schell-model beam," Phys. Rev. A **91**(1), 013823 (2015).
23. L. Ma and S. A. Ponomarenko, "Optical coherence gratings and lattices," Opt. Lett. **39**(23), 6656–6659 (2014).
24. L. Ma and S. A. Ponomarenko, "Free-space propagation of optical coherence lattices and periodicity reciprocity," Opt. Express **23**(2), 1848–1856 (2015).
25. Y. Chen, S. A. Ponomarenko, and Y. Cai, "Experimental generation of optical coherence lattices," Appl. Phys. Lett. **109**(6), 061107 (2016).
26. C. Liang, C. Mi, F. Wang, C. Zhao, Y. Cai, and S. A. Ponomarenko, "Vector optical coherence lattices generating controllable far-field beam profiles," Opt. Express **25**(9), 9872–9885 (2017).
27. S. Zhu, J. Wang, X. Liu, Y. Cai, and Z. Li, "Generation of arbitrary radially polarized array beams by manipulating correlation structure," Appl. Phys. Lett. **109**(16), 161904 (2016).
28. Y. Cai, Y. Chen, and F. Wang, "Generation and propagation of partially coherent beams with nonconventional correlation functions: a review," J. Opt. Soc. Am. A **31**(9), 2083–2096 (2014).
29. Y. Yuan, X. Liu, F. Wang, Y. Chen, Y. Cai, J. Qu, and H. T. Eyyuboglu, "Scintillation index of a multi-Gaussian Schell-model beam in turbulent atmosphere," Opt. Commun. **305**(15), 57–65 (2013).
30. S. Avramov-Zamurovic, C. Nelson, S. Guth, and O. Korotkova, "Flatness parameter influence on scintillation reduction for multi-Gaussian Schell-model beams propagating in turbulent air," Appl. Opt. **55**(13), 3442–3446 (2016).
31. F. Wang, X. Liu, Y. Yuan, and Y. Cai, "Experimental generation of partially coherent beams with different complex degrees of coherence," Opt. Lett. **38**(11), 1814–1816 (2013).
32. F. Wang, C. Liang, Y. Yuan, and Y. Cai, "Generalized multi-Gaussian correlated Schell-model beam: from theory to experiment," Opt. Express **22**(19), 23456–23464 (2014).
33. M. V. Hyde IV, S. Basu, D. G. Voelz, and X. Xiao, "Experimentally generating any desired partially coherent Schell-model source using phase-only control," J. Appl. Phys. **118**(9), 093102 (2015).
34. M. Hyde IV, S. Bose-Pillai, D. G. Voelz, and X. Xiao, "Generation of vector partially coherent optical sources using phase-only spatial light modulators," Phys. Rev. Appl. **6**(6), 064030 (2016).
35. S. Cho, M. A. Alonso, and T. G. Brown, "Measurement of spatial coherence through diffraction from a transparent mask with a phase discontinuity," Opt. Lett. **37**(13), 2724–2726 (2012).
36. J. K. Wood, K. A. Sharma, S. Cho, T. G. Brown, and M. A. Alonso, "Using shadows to measure spatial coherence," Opt. Lett. **39**(16), 4927–4930 (2014).
37. X. Liu, F. Wang, L. Liu, Y. Chen, Y. Cai, and S. A. Ponomarenko, "Complex degree of coherence measurement for classical statistical fields," Opt. Lett. **42**(1), 77–80 (2017).
38. S. W. Hell and J. Wichmann, "Breaking the diffraction resolution limit by stimulated emission: stimulated-emission-depletion fluorescence microscopy," Opt. Lett. **19**(11), 780–782 (1994).
39. M. J. Rust, M. Bates, and X. Zhuang, "Sub-diffraction-limit imaging by stochastic optical reconstruction microscopy (STORM)," Nat. Methods **3**(10), 793–795 (2006).
40. J. E. Oh, Y. W. Cho, G. Scarcelli, and Y. H. Kim, "Sub-Rayleigh imaging via speckle illumination," Opt. Lett. **38**(5), 682–684 (2013).
41. F. Tamburini, G. Anzolin, G. Umbriaco, A. Bianchini, and C. Barbieri, "Overcoming the Rayleigh criterion limit with optical vortices," Phys. Rev. Lett. **97**(16), 163903 (2006).
42. E. Mari, F. Tamburini, G. A. Swartzlander, Jr., A. Bianchini, C. Barbieri, F. Romanato, and B. Thidé, "Sub-Rayleigh optical vortex coronagraphy," Opt. Express **20**(3), 2445–2451 (2012).
43. G. A. Swartzlander, Jr., "Peering into darkness with a vortex spatial filter," Opt. Lett. **26**(8), 497–499 (2001).
44. D. Xu, X. Song, H. Li, D. Zhang, H. Wang, J. Xiong, and K. Wang, "Experimental observation of sub-Rayleigh quantum imaging with a two-photon entangled source," Appl. Phys. Lett. **106**(17), 171104 (2015).
45. M. G. L. Gustafsson, "Surpassing the lateral resolution limit by a factor of two using structured illumination microscopy," J. Microsc. **198**(Pt 2), 82–87 (2000).

Optics EXPRESS

46. M. G. L. Gustafsson, D. A. Agard, and J. W. Sedat, "Doubling the lateral resolution of wide-field fluorescence microscopy using structured illumination," Proc. SPIE **3919**, 141–150 (2000).
47. R. Heintzmann and C. Cremer, "Laterally modulated excitation microscopy: Improvement of resolution by using a diffraction grating," Proc. SPIE **3568**, 185–196 (1999).
48. J. W. Goodman, *Statistical Optics* (Wiley, 1985).
49. L. Mandel and E. Wolf, *Optical Coherence and Quantum Optics* (Cambridge University, 1995).
50. J. Garcia and R. Castandeda, "Spatial partially coherent imaging," J. Mod. Opt. **49**(13), 2093–2104 (2002).
51. R. Castañeda, "Phase space representation of spatially partially coherent imaging," Appl. Opt. **47**(22), E53–E62 (2008).
52. R. Betancur and R. Castañeda, "Spatial coherence modulation," J. Opt. Soc. Am. A **26**(1), 147–155 (2009).
53. Z. Tong and O. Korotkova, "Beyond the classical Rayleigh limit with twisted light," Opt. Lett. **37**(13), 2595–2597 (2012).
54. Y. Cai, X. Lu, and Q. Lin, "Hollow Gaussian beams and their propagation properties," Opt. Lett. **28**(13), 1084–1086 (2003).

1. Introduction

Coherence is one of the salient features of light, and it plays an important role in many applications, such as optical imaging [1–4], coincidence fractional Fourier transform [5], wavefront sensing [6], free-space optical communications [7, 8], optical scattering [9], information transfer and detection [10, 11], plasmonics [12–14], optical trapping and guiding [15, 16]. In recent years, there has been a growing interesting in partially coherent beams with prescribed correlation functions (i.e., degrees of coherence) due to their extraordinary properties displayed on propagation and on interacting with random media [17–37]. Gori et al. discussed the sufficient condition for devising a genuine correlation function of a partially coherent beam [18, 19]. A variety of partially coherent beams with prescribed correlation functions, such as non-uniformly correlated beams, multi-Gaussian correlated Schell-model beam, Laguerre-Gaussian correlated Schell-model beam, Hermite-Gaussian correlated Schell-model beam, optical coherence lattices, and so on, have been introduced theoretically and generated experimentally [4, 20–28]. One of the intriguing features of partially coherent beams with prescribed correlation functions is that such beams can produce a variety of nontrivial beam profiles in the far field [20–28], such as flat-top and dark-hollow beam profiles, beam arrays and lattices etc, which are expected to be useful in optical manipulation, material processing, image transmission and optical encryption. Furthermore, it was found that one can reduce turbulence-induced scintillation (i.e., intensity fluctuation) through manipulating the correlation functions of partially coherent beams [29, 30], which makes partially coherent beams with prescribed correlation functions attractive for free-space optical communications. Various methods have been developed to generate partially coherent beams with prescribed correlation functions and measure their correlation functions [17, 28, 30–37].

At the same time, the image resolution improvement in practical imaging systems is of great importance for imaging technology. Over the past decades, sub-Rayleigh resolution was achieved through improving image reconstruction techniques [38–40] or modulating the properties (e.g., amplitude and phase) of the illumination light [41–45]. It is known that the Rayleigh diffraction limit d_R is defined as the minimum resolvable distance between two points under incoherent light illumination. Some studies have shown that by modulating the phase of the illumination light, e.g. vortex phase, the separation distance of two equally luminous points may overcome the Rayleigh limit [41–44]. It was shown in [41] that a sub-Rayleigh separation distance about one order magnitude below the Rayleigh criterion can be achieved using two mutually incoherent overlapping optical vortices with different topological charges. Another technique to overcome the Rayleigh limit is to modulate the amplitude of the illumination light, i.e., structured illumination microscopy, which utilizes a spatially structured excitation light casting on the sample [45–47], and the resolution can overcome the diffraction limit by a factor of two. The relationship between image formation and spatial coherence of light has been explored in the past decades [48–53]. Castaneda developed a method for phase space representation of the image formation illuminated by partially coherent beams [51, 52]. In [53], Tong and Korotkova theoretically investigated the

Optics EXPRESS

image resolution of two points under illumination with a partially coherent beam carrying a twist phase, and the authors found that the maximum image resolution of $0.17d_R$ can in principle be attained by manipulating the twist phase. However, the twist phase of a partially coherent beam control still presents a challenge. Brown et al. explored the effect of partially correlated azimuthal vortex illumination (i.e., a special example of a vector partially coherent beam) on the image contrast [4], and the image resolution of about $0.93d_R$ was achieved, but it is direction/polarization dependent because the correlation function of the illumination beam is anisotropic.

In this paper, we analyze the image resolution using a telecentric imaging system with a low numerical aperture under partially coherent beam illumination with prescribed correlation function. We show that direction/polarization independent sub-Rayleigh image resolution can be achieved through manipulating the correlation function of the partially coherent beam; the resolution can in principle attain the value of $0.17d_R$. As an example, we analyze image resolution under Laguerre-Gaussian correlated Schell-model (LGCSM) beam illumination, and find that the image resolution equals to $0.85d_R$. Furthermore, we experimentally demonstrate sub-Rayleigh imaging of a 1951 USAF resolution target under LGCSM beam illumination.

2. Theoretical analysis

Consider an illumination field in the form of a partially coherent beam with prescribed correlation function, generated from a Schell-model source with the cross-spectral density (CSD) of the form [17, 18]

$$W(\mathbf{r}_1,\mathbf{r}_2)=\exp\left(-\frac{\mathbf{r}_1^2+\mathbf{r}_2^2}{4\sigma_0^2}\right)\mu(\Delta\mathbf{r}), \tag{1}$$

Here $\Delta\mathbf{r}=\mathbf{r}_2-\mathbf{r}_1$, $\mathbf{r}_i\equiv(x_i,y_i)$ represents an arbitrary point in the plane z = 0 and μ denotes the normalized correlation function (i.e., degree of coherence). In Eq. (1), we assumed that the partially coherent source intensity distribution is a Gaussian of the width σ_0.

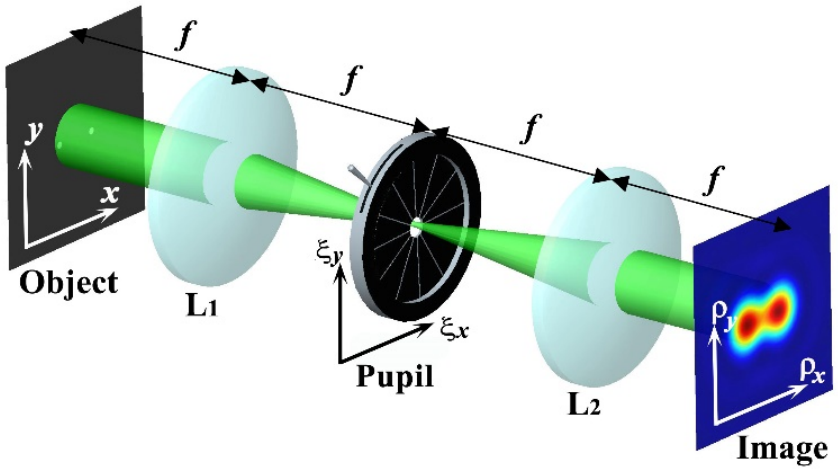

Fig. 1. Telecentric imaging system. Lenses L_1 and L_2 have the same focal length *f*.

Figure 1 shows a telecentric imaging system comprised of two thin lenses ($L_1$and L_2) and a pupil. The lenses $L_1$and L_2 have the same focal length *f*. The object and the pupil are located in the front and rear focal planes of L_1, and the image plane is located in the rear focal plane

Optics EXPRESS

of L_2. The CSD function of the field in the image plane is connected to that in the object plane by the following integral [44]

$$W(\boldsymbol{\rho}_1,\boldsymbol{\rho}_2)=\int W(\mathbf{r}_1,\mathbf{r}_2)O^*(\mathbf{r}_1)O(\mathbf{r}_2)h^*(\mathbf{r}_1,\boldsymbol{\rho}_1)h(\mathbf{r}_2,\boldsymbol{\rho}_2)d^2\mathbf{r}_1d^2\mathbf{r}_2, \tag{2}$$

where $O(\mathbf{r})$ is a transmittance function of the object, and $h(\mathbf{r},\boldsymbol{\rho})$ is an impulse function between the object plane and the image plane, given by

$$h(\mathbf{r},\boldsymbol{\rho})=-\frac{1}{\lambda^2 f^2}\int P(\boldsymbol{\xi})\exp\left(-\frac{ik}{f}\boldsymbol{\xi}\cdot(\mathbf{r}+\boldsymbol{\rho})\right)d^2\boldsymbol{\xi}. \tag{3}$$

Here $k=2\pi/\lambda$ is the wavenumber with λ being the wavelength, and $P(\boldsymbol{\xi})$ denotes the transmission function of the pupil. Suppose that the pupil is a circular aperture of radius R, then the impulse function reads

$$h(\mathbf{r},\boldsymbol{\rho})=-\frac{2\pi R^2}{\lambda^2 f^2}\frac{J_1(2\pi R|\mathbf{r}+\boldsymbol{\rho}|/\lambda f)}{2\pi R|\mathbf{r}+\boldsymbol{\rho}|/\lambda f}. \tag{4}$$

Here $J_1(\cdot)$ denotes the Bessel function of first kind of order 1. We assume the object to be an opaque screen with two small pinholes separated by a distance d, located symmetrically with respect to the y axis at y = 0. The transmittance function $O(\mathbf{r})$ of such an object can be approximately expressed in terms of two Dirac delta-functions as

$$O(\mathbf{r})=\delta(x-d/2,0)+\delta(x+d/2,0). \tag{5}$$

Substituting from Eqs. (1), (4) and (5) into Eq. (2), after integration and by setting $\boldsymbol{\rho}=\boldsymbol{\rho}_1=\boldsymbol{\rho}_2$, we obtain the intensity $S(\boldsymbol{\rho})$ in the image plane as

$$S(\boldsymbol{\rho})=\frac{1}{16\lambda^2 f^2}\left(\frac{\pi R^2}{\lambda f}\right)^2\exp\left(-\frac{d^2}{8\sigma_0^2}\right)\left[S_+^2+S_-^2+2\,\mathrm{Re}[\mu(d)]S_+S_-\right], \tag{6}$$

where

$$S_\pm=\frac{2J_1\left(2\pi R\sqrt{(\rho_x\pm d/2)^2+\rho_y{}^2}/\lambda f\right)}{2\pi R\sqrt{(\rho_x\pm d/2)^2+\rho_y{}^2}/\lambda f}. \tag{7}$$

Here "Re" denotes the real part. One finds from Eq. (6) that the image resolution of two points is closely determined by the third term, where the normalized correlation function μ plays a significant role. Note that the third term of Eq. (6) is dependent on the real part of the degree of coherence of the illumination light. Therefore, the phase of the degree of coherence could introduce the cosine-like modulation which may affect the image quality. In real situation, we could use the illumination light whose degree of coherence is real to avoid phase modulation. Furthermore, the third term of Eq. (6) is sensible to differences of the illumination of the pinholes, and non-uniform illuminations will limit the control ability of the coherence degree to affect the image. Thus, the control of the degree of coherence and the intensity distribution of the illumination light are very important. In experiment, it is easy to generate a partially coherent illumination light with uniform-intensity (i.e., free of speckles) [17]. The degree of coherence and the intensity distribution of the illumination light can be controlled independently. Therefore, the effect of the non-uniform illumination on the image quality can be neglected.

Optics EXPRESS

Under the condition of incoherent light illumination, i.e., $\mu(\Delta\mathbf{r}) = \delta(\Delta\mathbf{r})$, the third term in the square brackets in Eq. (6) vanishes yielding the classical Rayleigh limit (i.e., the minimum resolvable distance between two pinholes), i.e., $d_R = 0.61\lambda f / R$. In this case, the ratio of the intensity at the image center to the maximum intensity is about 0.735, i.e., $S(0)/[S(\boldsymbol{\rho})]_{\max} = 0.735$. If the illumination field is a conventional partially coherent beam, i.e., Gaussian Schell-model (GSM) beam, whose normalized correlation function is expressed as $\mu(\Delta\mathbf{r}) = \exp\left(-\Delta\mathbf{r}^2/2\delta_0^2\right)$ with δ_0 being the spatial coherence width (SCW), the image resolution monotonously decreases as δ_0 increases because μ always takes a non-negative value for any $\Delta\mathbf{r}$.

If the illumination field is a nonconventional partially coherent beam whose normalized correlation function can take on negative values, the image resolution of two pinholes can overcome the classical Rayleigh limit and attain the magnitude of $0.17d_R$ whenever the degree of coherence attains its minimum equal to -1. As an example, we assume the illumination field to be an LGCSM beam (i.e., a typical example of partially coherent beam with a prescribed correlation function), whose normalized correlation function takes the following form

$$\mu(\Delta\mathbf{r}) = L_n^0\left(\frac{\Delta\mathbf{r}^2}{2\delta_0^2}\right)\exp\left(-\frac{\Delta\mathbf{r}^2}{2\delta_0^2}\right), \tag{8}$$

Here L_n^0 denotes a Laguerre polynomial with the radial index n and azimuthal index 0. When $n = 0$, the LGCSM beam reduces to a GSM beam.

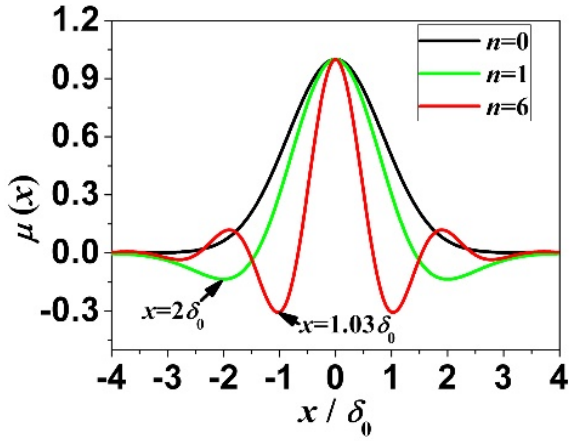

Fig. 2. Variation of the $\mu(x)$ of an LGCSM beam with x/δ_0 for different values of n.

Figure 2 shows the distribution of $\mu(x)$ of an LGCSM beam versus x/δ_0 for different values of n. Notice that unlike $\mu(x)$ of a GSM source ($n = 0$), $\mu(x)$ of an LGCSM source exhibits oscillations as a function of x. When $\mu(x)$ at $x = d$ just attains its minimum value by adjusting the magnitude of δ_0, the third term at $\boldsymbol{\rho} = 0$ also attains its minimum value which is negative, then the image resolution of two points can be improved beyond the Rayleigh limit (i.e., incoherent light illumination). An attractive feature of our illumination scheme is image resolution isotropy—the resolution does not depend on the specified positions of two pinholes

Optics EXPRESS

in the object plane. This important feature distinguishes our approach from that of Ref [53]. In our case, the SCW δ_0 plays an important role for sub-Rayleigh resolution realization. As shown in Fig. 2, the value of δ_0 required to achieve the best resolution depends on the index n.

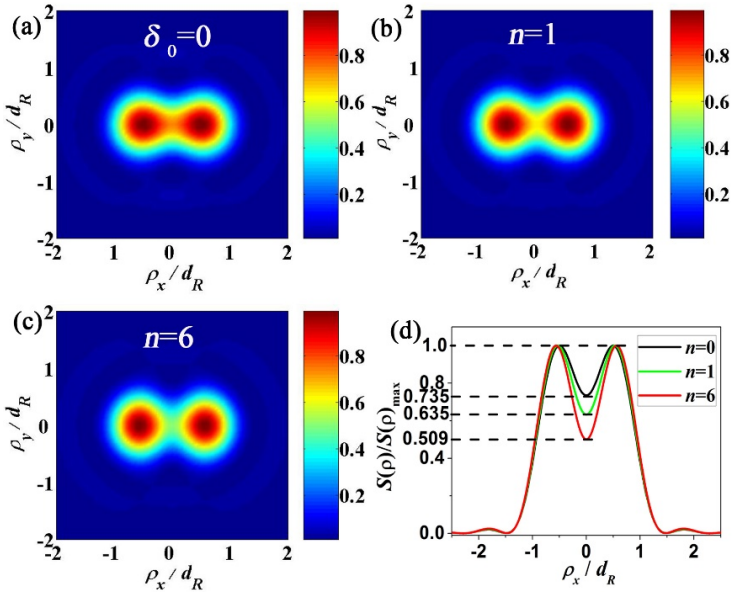

Fig. 3. Images of two pinholes with separation $d = d_R$ under the illumination of (a) an incoherent source; (b) an LGCSM source with n = 1 and $\delta_0 = 0.5d_R$; (c) an LGCSM source with n = 6 and δ_0=0.98d_R . The corresponding cross lines ($\rho_y = 0$) of the images are shown in Fig. 3(d).

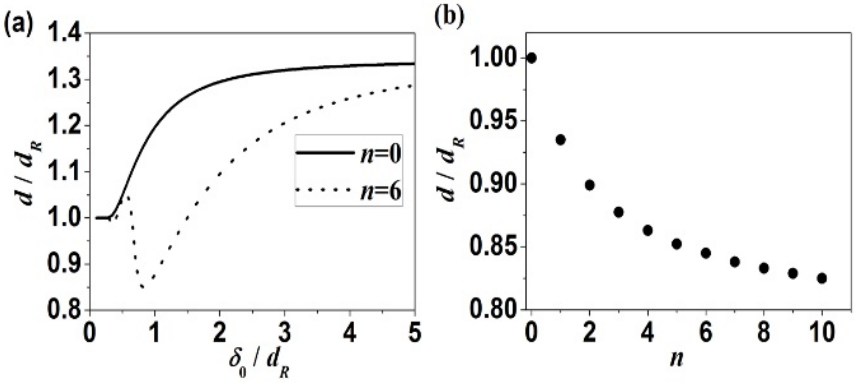

Fig. 4. (a) Resolvable separation between two pinholes versus δ_0 / d_R; (b) Minimum resolvable separation between two pinholes versus radial index n.

Figure 3 illustrates the image of two pinholes with $d = d_R$ under incoherent source illumination (n = 0, δ_0 = 0), as well as under that of an LGCSM source with n = 1 and 6. As expected, the image of two pinholes is barely resolvable under incoherent light illumination. However, under LGCSM source illumination with $\delta_0 = 0.5d_R$ for n = 1 or $\delta_0 = 0.98d_R$ for n =

Optics EXPRESS

6, the image of two pinholes can be resolved, i.e., the normalized intensity at the central point is greatly reduced [see Fig. 3(d)]. We point out that to resolve two points with a sub-Rayleigh separation, δ_0 is not required to exactly equal to its critical value. It is sufficient for it to lie in a vicinity of this value. To elucidate the influence of δ_0 on the image resolution of two points, we plot in Fig. 4(a) the resolvable separation between two pinholes versus δ_0. As expected, the resolvable separation increases with δ_0 for GSM beam ($n = 0$) illumination. For LGCSM beam illumination with $n = 6$, about 10% smaller than the Rayleigh diffraction limit can be achieved when the SCW is in the range from $0.72d_R$ to $1.1d_R$. The resolvable separation of two pinholes reaches its minimum value, $d \approx 0.85d_R$ when $\delta_0 \approx 0.82d_R$. The dependence of the minimum resolvable separation on the index n is shown in Fig. 4(b). We find that as n increases, the ability to distinguish two pinholes is enhanced because the minimum value of μ decreases as n increases.

3. Experimental verification

We carry out an experiment to demonstrate sub-Rayleigh imaging under LGCSM beam illumination. Figure 5 shows the experimental setup for generating an LGCSM beam and demonstrating sub-Rayleigh imaging. The setup for generating an LGCSM beam is similar to that reported in [31]. A linearly polarized in the x-direction Nd: YAG laser ($\lambda = 532$nm) beam is transmitted through a beam expander and a beam splitter (BS). The reflected beam from the BS propagates toward a spatial light modulator (SLM) which can be regarded as a computer-controlled phase screen used to produce the beam with prescribed beam profile. In order to generate a LGCSM beam in the object (OB) plane, the beam produced by the SLM should be a hollow Gaussian beam with its electric field being [54]

$$E(\mathbf{v}) = \left(\frac{|\mathbf{v}|}{\omega_0}\right)^n \exp\left(-\frac{\mathbf{v}^2}{\omega_0^2}\right), \tag{9}$$

where $\mathbf{v} \equiv (v_x, v_y)$ denotes the position vector, n and ω_0 are the beam order and beam width, respectively. The pattern of the phase screen loaded on the SLM for generating a hollow Gaussian beam is obtained by computing the interference pattern between a plane wave (reference wave) and a hollow Gaussian beam. After reflecting from the SLM, the first-order diffraction beam from the SLM can be considered as a hollow Gaussian beam. Then a circular aperture (CA_1) and a thin lens (L_1) are used to block the other unwanted diffraction orders except the first-order diffraction and imaging the hollow Gaussian beam onto a rotating ground-glass disk (RGGD) plane, respectively. The transmitted beam from the RGGD becomes an incoherent light with Gaussian statistics, and then is collimated by a collimating lens L_2 with focal length f_2. By applying the Van Cittert-Zernike theorem [49], the normalized correlation function of the beam behind the L_2 can be expressed as

$$\mu(\Delta\mathbf{r}) \propto \int I(\mathbf{v}_1) \exp\left[-\frac{i2\pi\mathbf{v}_1 \cdot \Delta\mathbf{r}}{\lambda f_2}\right] d^2\mathbf{v}_1, \tag{10}$$

where $I(\mathbf{v}_1)$ is the intensity distribution of the hollow Gaussian beam on the RGGD plane. Substituting Eq. (9) into Eq. (10) and after integration, we obtain $\mu(\Delta\mathbf{r}) = L_n^0\left(\Delta\mathbf{r}^2/2\delta_0^2\right)\exp\left(-\Delta\mathbf{r}^2/2\delta_0^2\right)$, which is known as the normalized correlation function of the LGCSM beam described in section 2. The coherence width is obtained as $\delta_0 = \lambda f_2 / \omega_0$ if we assume that the designed beam width of the hollow Gaussian beam equals to that on the RGGD plane. In our experiment, the coherence width is controlled by adjusting

Optics EXPRESS

the beam width ω_0 through changing the phase screen loaded on the SLM. The Gaussian amplitude filter (GAF) located behind L_2 is used to transform the beam profile to Gaussian shape. To generate a GSM beam, we replace the SLM with a reflecting mirror in Fig. 5. The normalized correlation function μ and the corresponding δ_0 are measured by the method introduced in [28, 31]. When the LGCSM or GSM beam is produced, it serves as illumination light in the telecentric imaging system. The focal lengths of lenses L_3 and L_4 are $f_3 = f_4 = f =$ 250mm, and the radius of the iris (CA_2) is R = 1.5mm. On the basis of the Rayleigh criterion, the minimum resolvable separation of two points in our image system is $d_R = 54.2\mu m$. A charge-coupled device (CCD) with single pixel $4.6\mu m \times 4.6\mu m$ is placed in the image plane to record an image of the object (i.e., 1951 USAF resolution target). The integration time of the CCD is set as 100ms.

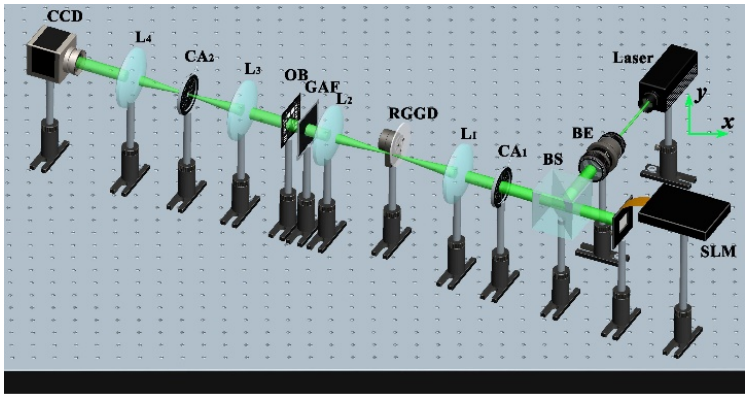

Fig. 5. Experimental setup for generating an LGCSM beam and demonstrating sub-Rayleigh imaging. Laser, ND: YAG laser; BE, beam expander; BS, beam splitter; SLM, spatial light modulator; CA_1, CA_2, circular apertures; L_1, L_2, L_3, L_4, thin lenses; RGGD, rotating ground-glass disk; GAF, Gaussian amplitude filter; OB, 1951 USAF resolution target; CCD, charge-coupled device.

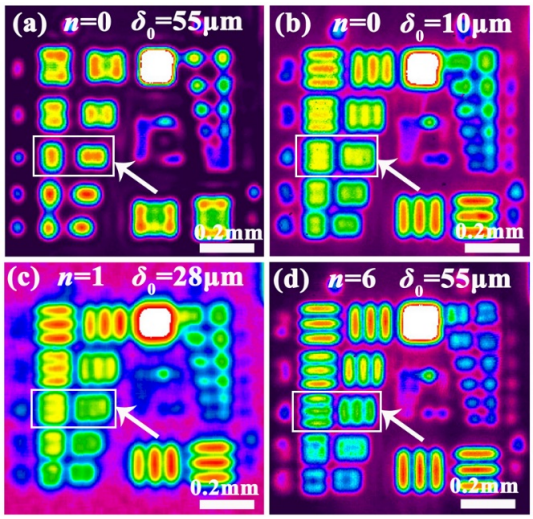

Fig. 6. Image of the target under the illumination of (a) a GSM beam with δ_0 = 55um; (b) a GSM beam with δ_0 = 10um; (c) an LGCSM beam with n = 1, δ_0 = 28um; (d) an LGCSM beam with n = 6, δ_0 = 55um.

Optics EXPRESS

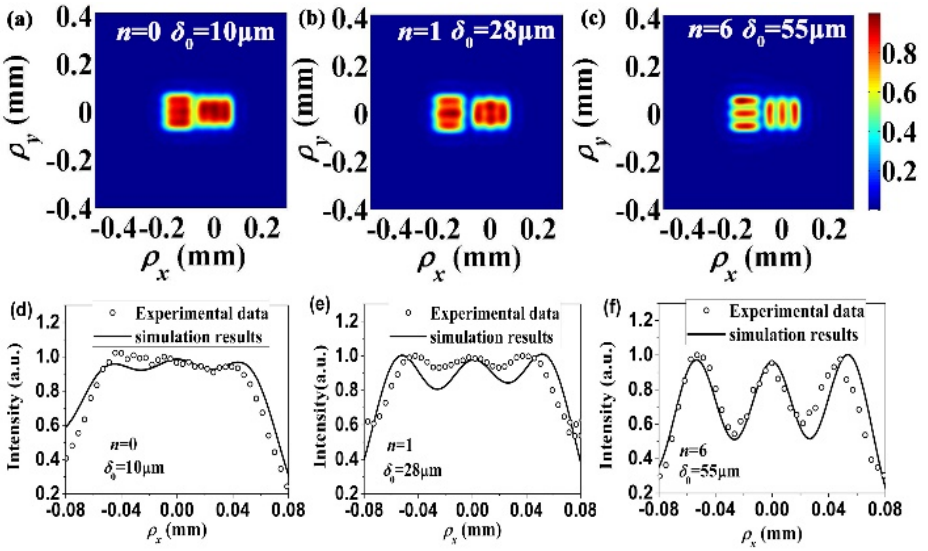

Fig. 7. (a)-(c) Simulation results of the image of the area in rectangular box shown in Fig. 6 under the illumination of different beams; (d)-(f) the corresponding cross lines of simulation results (solid line) and experimental results (circular dots) of the right side triple-slit at $\rho_y = 0$.

The experimental results of the 1951 USAF resolution target image, captured by the CCD, are shown in Fig. 6. For the GSM beam illumination ($n = 0$) case, one finds that although the image resolution for $\delta_0 = 10\mu m$ is better than that for $\delta_0 = 55\mu m$, the area inside the rectangular box indicated by a white arrow could not be clearly distinguished. According to the target, the indicated area consists of two triple-slits with the slit width and separation being $24.8\mu m$ and $49.6\mu m$, respectively, i.e., segment 4-3 in the test target. For the LGCSM beam illumination case, the image of the two triple-slits indicated by the white arrow becomes progressively more resolvable as the index n increases, implying that sub-Rayleigh image resolution is realized. Wave optics numerical simulation results of segment 4-3, illuminated by different types of beams, are shown in Fig. 7(a)-7(c). One sees that the image resolution is indeed improved under LGCSM beam illumination with $n = 6$ and $\delta_0 = 55\mu m$. Our numerical results (not presented) also show that the image resolution under incoherent light illumination is almost the same as that under GSM beam illumination with $\delta_0 = 10\mu m$. The corresponding cross lines of simulation results (solid line) and experimental results (circular dots) of the right side triple-slit at $\rho_y = 0$ are shown in Fig. 7(d)-(7f). One finds that except the case of $n = 6$ and $\delta_0 = 55\mu m$, there are slight deviations between the experimental results and the theoretical results [see Fig. 7(d) and 7(e)]. This deviations may be due to the imperfect modulation of the normalized correlation function in the experiment, i.e., the minimum value of $\mathrm{Re}[\mu(d)]$ in the experiment did not reach the minimum value predicted by the theory. In addition, the unwanted scattering light and the aberration in the image system also deteriorate the image resolution. However, in general, our experimental results agree reasonably well with our numerical results.

4. Summary

We summarize by saying that we analyzed the image of two pinholes in a telecentric imaging system under partially coherent beam with prescribed correlation function illumination. We have found that the image resolution, which is independent of precise positions of two

Optics EXPRESS

pinholes in the object plane, can overcome the classical Rayleigh diffraction limit d_R via controlling the source correlation function. Furthermore, we have demonstrated experimentally the sub-Rayleigh imaging of a 1951 USAF resolution target under LGCSM beam illumination. The minimum image resolution achieved with LGCSM beam illumination is about $0.85d_R$, while its value can in principle reach $0.17d_R$, provided it is illuminated by a partially coherent beam with the correlation function μ attaining a minimum value of -1. Our prediction motivates us to design and generate such partially coherent beams in the future. Our results are useful for optical imaging and may find applications to high-resolution microscopy.

Funding

National Natural Science Fund for Distinguished Young Scholar (11525418); National Natural Science Foundation of China (NSFC) (11474213, 11604264); Project of the Priority Academic Program Development of Jiangsu Higher Education Institutions; Natural Science Basic Research Plan in Shanxi Province of China (2016JQ1021); Postgraduate Research & Practice Innovation Program of Jiangsu Province (KYCX17_2024).